The Meteoritical Society

Meteoritics & Planetary Science 57, Nr 12, 2216–2228 (2022)
doi: 10.1111/maps.13924

Once in a summer: Fall history of the JaH 073 strewn field, Sultanate of Oman

Karl WIMMER[1]*, Edwin GNOS[2], and Beda A. HOFMANN[3]

[1]Salvatorgasse 12, 86720 Nördlingen, Germany
[2]Muséum d'histoire naturelle de la Ville de Genève, 1208 Geneva, Switzerland
[3]Naturhistorisches Museum der Burgergemeinde Bern, 3005 Bern, Switzerland
*Corresponding author. E-mail: karl-wimmer@t-online.de

(Received 08 June 2022; revision accepted 17 October 2022)

Abstract–Modeling of a prehistoric fall can be successful if a strewn field is very well documented and coordinates, masses, and shapes of all individual stones are recorded. In combination with meteoroid mass and wind model constraints, a detailed scenario of the atmospheric passage is obtained for the ~20 × 6 km-sized JaH 073 L6 strewn field in Oman. The wide mass ranges from 52.2 kg to <1 g together with the large number of ~3500 stones offer the statistical basis to reconstruct the trajectory and the fragmentation sequence. The size of the meteoroid, constrained by noble gas analyses, corresponds to an initial mass of about 12 t at atmospheric entry using an L-chondrite bulk density of 3400–3500 kg m^{-3}. Assuming typical ablation behavior, these data are compatible with an entry velocity of 20 ± 3 km s^{-1}. The best model fit is achieved for a serial fragmentation scenario starting at an altitude of ~34 km and showing a main fragmentation at 26 km. A resolved event seems to have occurred at 22 km, followed by a more diffuse fragmentation at 19 km. The vertical trajectory angle is calculated at 43 ± 2° and the azimuth at 329 ± 1°. The position of numerous outlying meteorites in the strewn field can only be reproduced by repeated fragmentation with cumulated transverse velocities from explosive events. The wind model adopted from modern data fits surprisingly well and indicates summer monsoon with strong easterly winds during the fall event, consistent with paleoclimatic data.

INTRODUCTION

There is quite a number of strewn field producing meteorite falls for which accurate tracking data on atmospheric passage are available and where material was recovered on the ground. In addition to the 13 falls as compiled in Popova et al. (2011), several more recent falls including the most spectacular event of Chelyabinsk in 2013 (e.g., Borovička et al., 2013; Buhl & Wimmer, 2013; Emel'Yananko et al., 2014; Popova et al., 2013; Trigo-Rodríguez et al., 2021) could be evaluated.

The continued work of the Czech part of the European Fireball Network and more recent installations in North America, Australia, and Europe, for example, the Global Fireball Observatory (Devillepoix et al., 2020) and the global FRIPON camera network (Colas et al., 2020), have helped to increase the number of falls recovered with the aid of all-sky fireball cameras to over 40. The tracking data, obtained with video devices and by meteorite tracking networks (e.g., Ceplecha, 1961; Devillepoix et al., 2022; Halliday, 1971; Jenniskens et al., 2019; Oberst et al., 1998; Spurný et al., 2009), show that more than 90% of the meteoroids undergo atmospheric fragmentation (e.g., Ceplecha et al., 1993). Although meteorite tracking observations have considerably increased the number of fresh meteorite recoveries on the ground, only few, for example, Bunburra Rockhole (Bland et al., 2009; Spurný et al., 2012) and Almahata Sitta (Jenniskens et al., 2009), fell in relatively flat desert regions, where a nearly 100% recovery of fragments on the ground is feasible. Complete recovery is impossible in rugged and/or vegetation-covered terrains.

These cases prove that different modeling algorithms using data extracted from meteorite tracking (speed, deceleration, light flares, or sound registrations), in combination with an atmospheric density gradient model and high-altitude wind data, can successfully

predict a probability field for meteorites on the ground. The position of an individual meteorite within the probability field, however, depends on additional effects that are in most cases not accessible by visual tracking data. First, there is the potentially high transverse velocity component resulting from sometimes strong explosions upon fragmentation. Second, there is the wind drift during the dark flight in the lower atmosphere after the meteorite is sufficiently decelerated to stop emission of light by collision with atmospheric molecules. The exposure to the wind may last for a few minutes and cause strong displacement; it is dependent on mass and especially the shape of the fragment. Irregular shapes can cause deflections in all directions including uplift. Thus, each meteorite recovered on the ground with well-documented data helps to improve the knowledge on aerodynamic drag and shape factors and to shed light on the fragmentation mechanism.

There exist many historic and prehistoric strewn fields, for example, L'Aigle (Biot, 1803), Allende (Clarke et al., 1970), Camel Donga (Cleverly et al., 1986), Campo del Cielo (Wright et al., 2006), Jilin (Jilin Consortium Study, 1985), Holbrook (Foote, 1912), Mbale (Jenniskens et al., 1994), Millbillillie (Moore et al., 1999), Mócs (Koch, 1882), Mundrabilla (De Laeter, 1972; De Laeter & Cleverly, 1983), Murchison (Fuchs et al., 1973), Norton County (LaPaz, 1965), Park Forest (Simon et al., 2004), Sikhote Alin (Krinov, 1966) and strewn fields in Antarctica (e.g., Welten et al., 2011), consisting of hundreds to thousands of individual stones. The number of finds is often well known; in many cases, the mass of individual stones is known too, but in most cases, the exact find location and especially the shape of stones is not reported. Thus, important data permitting detailed modeling of historic and prehistoric falls are missing.

In contrast, recent meteorite search activities in hot deserts produced excellent data sets of large undisturbed prehistoric strewn fields. These include, for example, the Gold Basin L4 strewn field in the United States (Kring et al., 2001); the DaG CO3 strewn field in Libya (Schlüter et al., 2002); and the ordinary chondrite strewn fields SaU 001 (L4/5; Grossman, 2000), JaH 073 (L6; Gnos et al., 2009; Huber et al., 2008), and JaH 091 (L5; Gnos et al., 2006) in the Sultanate of Oman. In all these cases, mass, coordinates, and even shape factors of most individual stones are known or accessible.

While the prediction of meteorite fall areas from luminous trajectory data is a well-established practice nowadays, the reconstruction of meteors from strewn field data is little explored.

In this study, we use a modeling approach considering the geographic location, and in selected cases also the shape of the stones in order to obtain a more detailed scenario of the prehistoric atmospheric passage of the JaH 073 fireball.

The JaH 073 Strewn Field

The Jiddat al Harasis (JaH) 073 L6 (S4W2-4) strewn field was discovered on January 17, 2002 in the Sultanate of Oman and covers an area of 20 × 6 km (Gnos et al., 2009) (Fig. 1). The almost 3500 single stones recovered range in mass from 52.2 kg down to <1 g (total collected mass about 600 kg; see Data S1 in supporting information). The strewn field is NNW–SSE oriented, indicating an atmospheric entry from SE at intermediate angle relative to the surface. The strewn field shows a deflection to the west at its lower mass end. Two gentle depressions containing deposits of sand, clay, and silt cover small sections of the strewn field (Gnos et al., 2009). Although complete collection could not be achieved in these sections, we estimate that most large (>1 kg) and approximately 60%–80% of smaller stones have been collected, corresponding to >90% of the total mass. However, when studying the distribution of stones in the JaH 073 strewn field, large empty areas are recognizable in between stringers of stones on the western side of the curved strewn field axis (Fig. 1). Intense additional searching at the small mass end has shown that still some of these irregularities may be related to incomplete sampling. Although the strewn field as a whole appears to be mass sorted, the mass group diagram shown in Fig. 2 shows clearly a strong overlap of mass groups. Moreover, Gnos et al. (2009) mentioned a 741 g stone (0201-1130) located north of the largest mass of 52.2 kg. This stone has a slightly platy shape (11 × 9.5 × 4.5 cm; Fig. 3). Additional search campaigns based on the first modeling results revealed three additional stones (0902-84, 39.1 g; 0902-85, 169.6 g; 0902-86, 5800 g) in the vicinity of the proposed fall line to the North of the strewn field (Figs. 1 and 2). Two of them (0902-85 and 0902-86) separated by some 118 m are parts of one stone as confirmed by shape matching.

Of course, one cannot rule out that some stones could have been displaced by humans. However, with the exception of a pile made in place from a large, fragmented meteorite as a driving indicator for Bedouins, we have not found evidence of human activity. Bedouins only crossed these areas after strong rains, but they mainly stayed in dunes where vegetation is more abundant after rain. Displacement by wind can also be ruled out. This is evident from weathered meteorites on slopes, where the fragments are found dispersed within a few meters. We also exposed cut and weighted peridotites in an area of strong wind for several years. The stones showed measurable weight losses due to wind ablation, but they remained in position. In some areas, wind ablation is

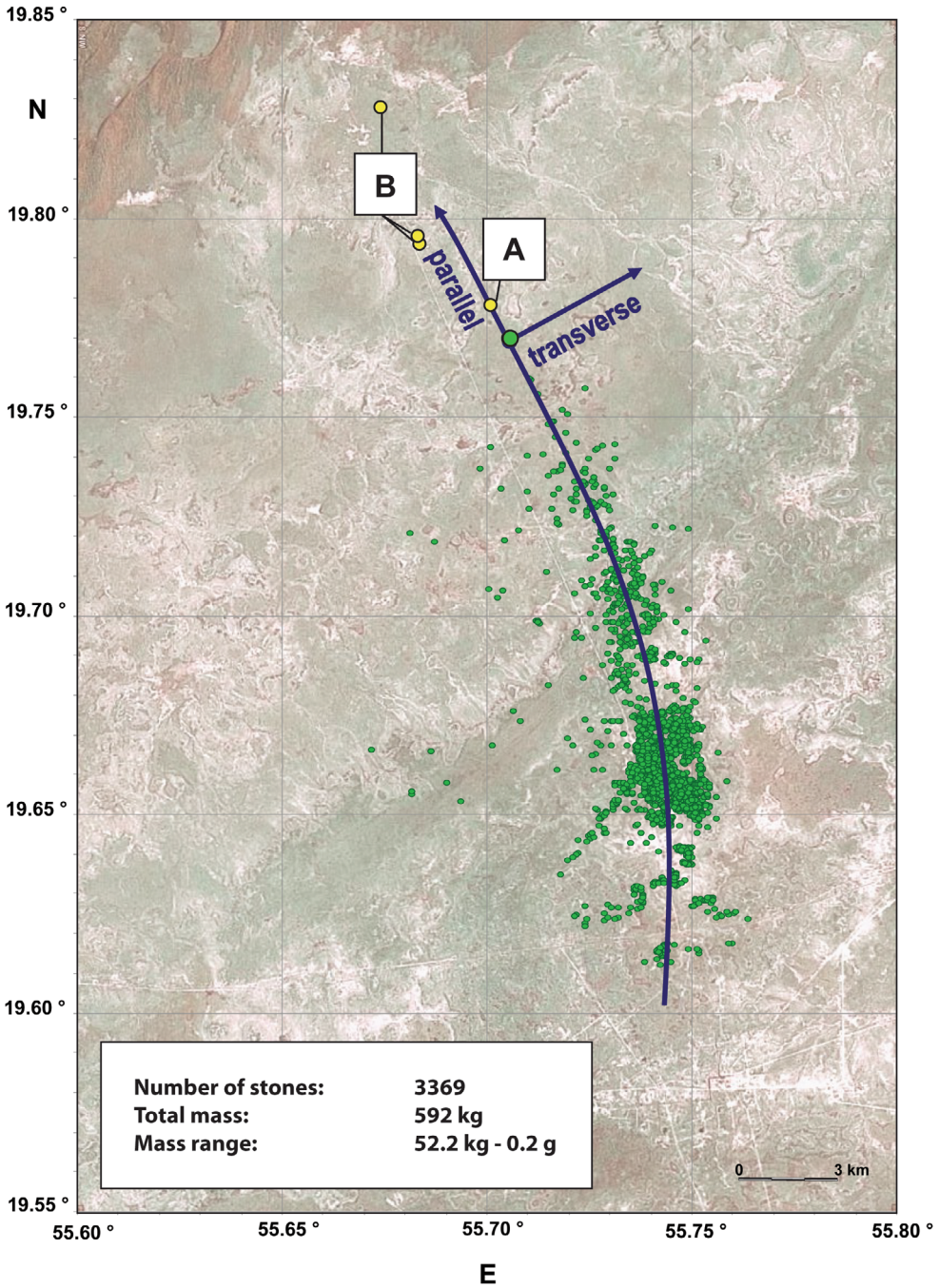

Fig. 1. JaH 073 strewn field. Note the curved center line defined by mass group center points. It will serve as the "parallel" axis of an adjusted coordinate system with zero point at the main mass introduced for the further analysis. A and B indicate locations of selected outliers. (A) 0201-1130 (741 g); (B) 0902-84 (39.1 g), 0902-85 (169.6 g), and 0902-86 (5800 g). (Color figure can be viewed at wileyonlinelibrary.com.)

strong and meteorites and limestones develop striations on the upper side indicating the predominant direction of the wind. In such cases, a turned object is easily recognizable.

JaH 073 samples gave a ^{14}C fall age of 18.1 ± 2.7 ka (Sliz et al., 2022). The meteorite seems not to be saturated in ^{10}Be, which resulted in the underestimated age of 14.4 ka reported earlier by Gnos et al. (2009). Huber et al. (2008) measured the concentrations and isotopic compositions of He, Ne, and Ar in 11 different strewn field fragments ranging from <100 g to >50 kg, including seven samples from known locations (drill cores) within the main mass. They also measured the concentrations of cosmogenic

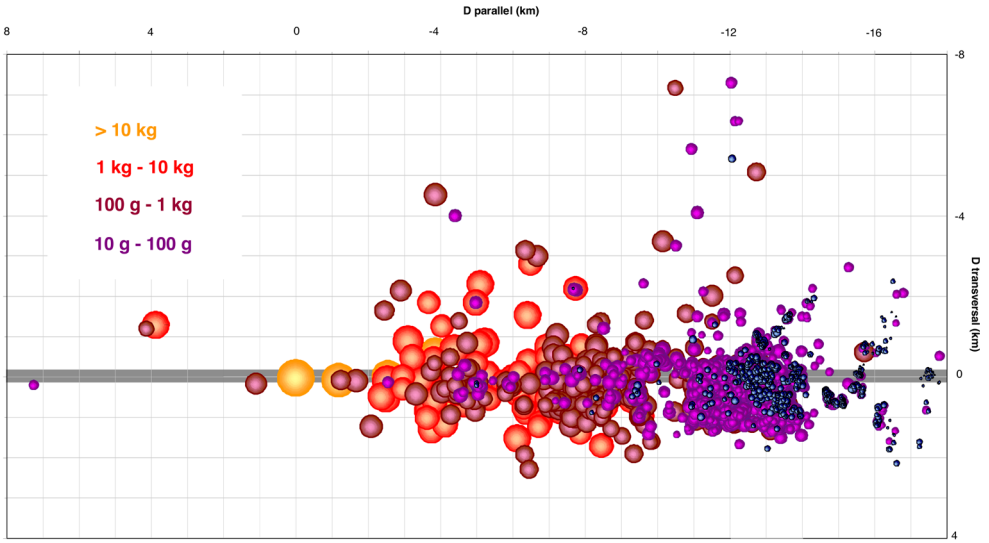

Fig. 2. Mass groups in adjusted coordinates; note the large overlap in parallel direction and the biased distribution in transverse direction. (Color figure can be viewed at wileyonlinelibrary.com.)

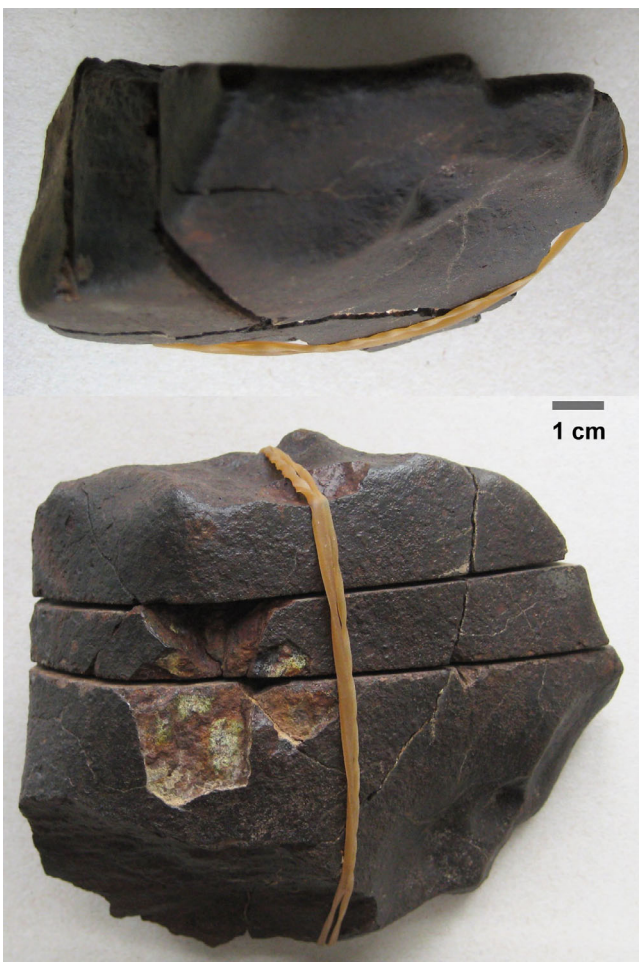

Fig. 3. Meteorite 0201-1130 (741 g). Note the disk-like shape. (Color figure can be viewed at wileyonlinelibrary.com.)

^{10}Be, ^{26}Al, ^{36}Cl, and ^{41}Ca in 10 samples. The cosmogenic nuclide data showed that, like other large chondrites studied, JaH 073 experienced a complex exposure history. Integrating all data, they obtained a consistent history with a first-stage exposure of ~65 Ma within ~20 cm of the surface of the L-chondrite parent body, followed by ejection of a 1.5–2 m large object, which was then delivered to Earth within about 0.5 and 0.7 Ma. This information will be used in this study to constrain the initial mass of the meteoroid.

METHODS

Modeling Approach

A fall reconstruction for 100% of the individual stones is impossible based on the two-dimensional strewn field pattern, but simplified scenarios can be derived depending on the number of resolvable substructures of the strewn field. Not all model parameters are independent, thus causing ambiguities in all scenarios (e.g., meteoroid mass loss and velocity are strongly correlated). However, in this particular case, the size of the meteoroid estimated from cosmic nuclide data together with the well-known total meteorite mass on the ground provides additional constraints. The modeling approach is therefore to start with the simplest single-fragmentation model and to iteratively progress to more complex scenarios. Therefore, we extend the standard single-body algorithm (Ceplecha et al., 1998) and use experimentally found drag and shape factors (Wimmer, 2009).

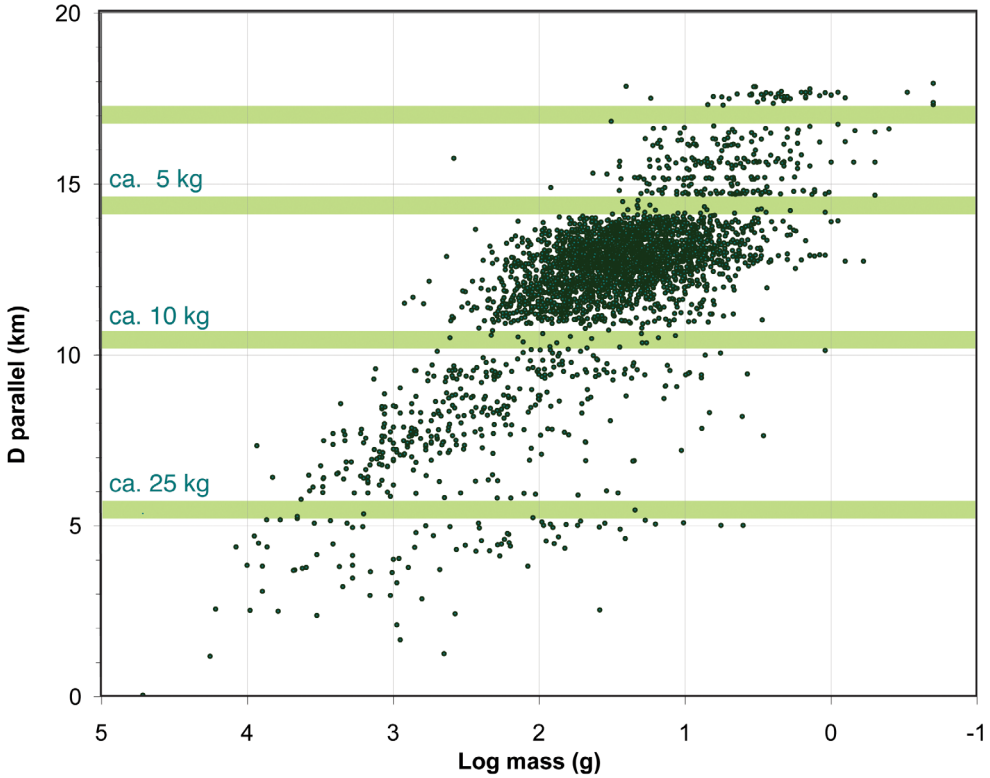

Fig. 4. Logarithmic mass distribution along the strewn field; note the gaps caused by geographic features; for modeling, the lost masses are estimated by interpolation. (Color figure can be viewed at wileyonlinelibrary.com.)

Analysis of Meteorite Mass Distribution and Estimate of Initial Meteoroid Mass

For the analysis of the mass distribution, we introduce an adjusted coordinate system with a curved axis through the strewn field, which is defined by the mass group center points, and a "transverse" direction always normal to it (Fig. 1). This system is thought to ease the separate study of mass mixing in the two orthogonal directions (Fig. 2) and is the basis for the subsequent diagrams (Figs. 4 and 5).

As mentioned in Gnos et al. (2009), the JaH 073 strewn field has some geographic features such as sandy depressions leading to incomplete sampling. The logarithmic mass distribution along the strewn field axis (Fig. 4) shows the respective gaps and allows interpolative correction. Some small discontinuities may, beyond statistics, reflect unfavorable search conditions in minor areas. The smooth envelope curve in Fig. 5 tries to include all these deficits, resulting in an extrapolated total mass of 700 kg, which may be taken as the maximum of a one-sided probability distribution with decreasing probabilities toward lower mass values. The "true" value may be somewhere in between 640 and 700 kg. For the further analysis, we adopt a conservative estimate of 650 kg.

The detailed analysis of cosmogenic nuclides in JaH 073 by Huber et al. (2008) constrains the initial meteoroid diameter to 1.5–2 m. In combination with unaltered chondrite bulk density data of ~3.5 g cm^{-3} (e.g., Britt & Consolmagno, 2003), this corresponds to an initial mass of about 12,000 kg. The uncertainty, however, is considerable due to the unknown shape of the meteoroid; it may be as large as a factor 2.

Atmospheric Entry Velocity

The strewn field does not yield straightforward information on the fall dynamics. In order to get a rough constraint for the entry velocity, we use the mass loss during the atmospheric passage.

The meteoroid ablation increases theoretically with the third power of the velocity (Ceplecha et al., 1998) with an apparent ablation coefficient of 0.014 s^2 km^{-2} taken as typical for ordinary chondrites. Starting from a range of 6–24 t mass at atmospheric entry and ending with 650 ± 50 kg on the ground, we derive an entry velocity in the range of 17–23 km s^{-1} (20 ± 3 km s^{-1}; Fig. 6). In the further scenario development, we adopt a rounded model value of 20 km s^{-1}. Apparent ablation higher than normal due to more violent fragmentation might lead to velocities closer to the lower end of the

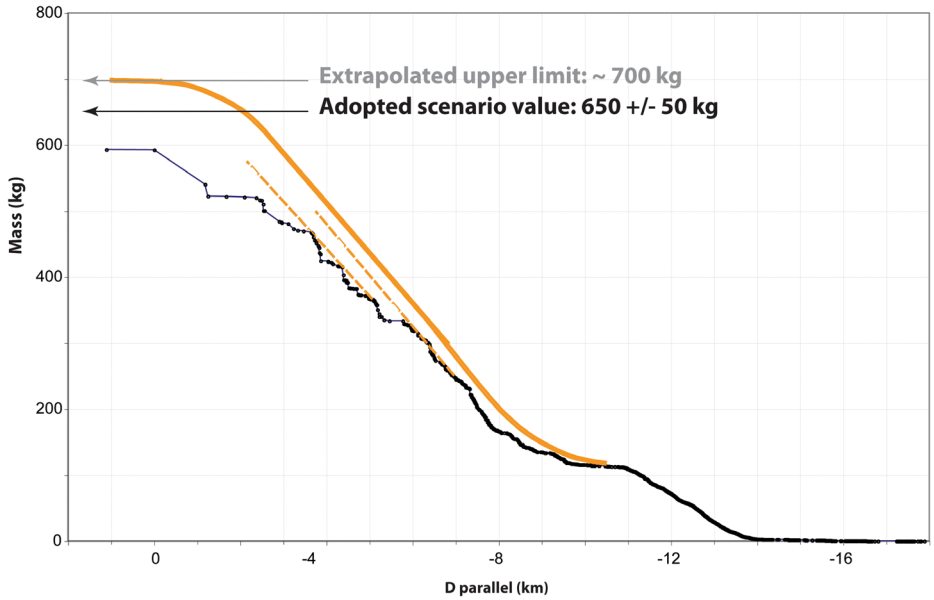

Fig. 5. Estimate of the total meteorite mass by interpolation and extrapolation, bridging the gaps caused by incomplete sampling. A conservative estimate of 650 ± 50 kg is adopted for the scenario. (Color figure can be viewed at wileyonlinelibrary.com.)

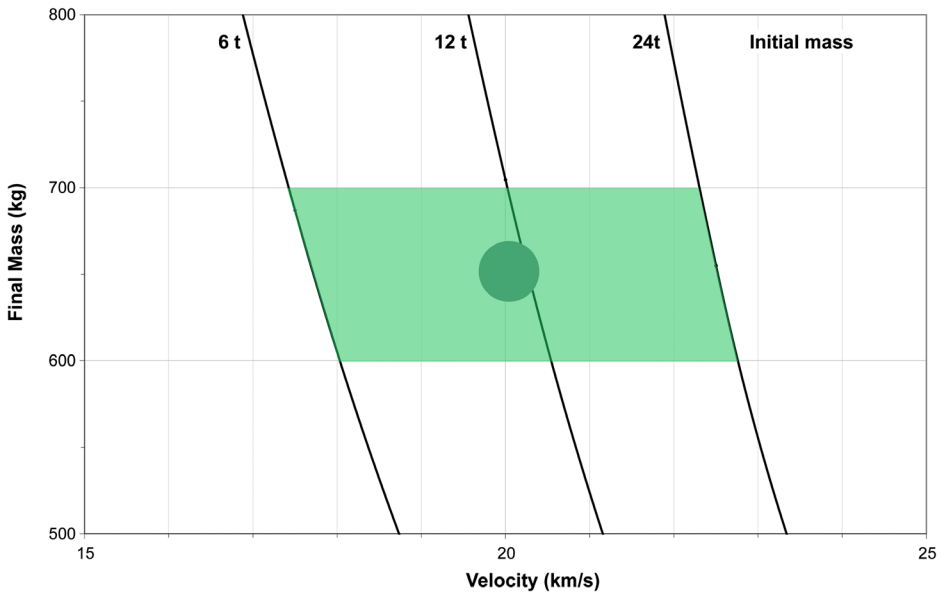

Fig. 6. Final total meteorite mass resulting from different initial meteoroid masses and atmospheric entry velocity (with apparent ablation coefficient 0.014 s^2 km^{-2} for ordinary chondrites). An increased ablation coefficient, to account for stronger fragmentation, results in a shift toward lower velocities with minor influence on the geometry of the strewn field (see discussion). (Color figure can be viewed at wileyonlinelibrary.com.)

range with little impact, however, on the geometric model parameters (see discussion).

Wind Model

As the JaH 073 fall happened some 18.1 ka ago (Sliz et al., 2022), there is no direct information about the wind situation during fall time. The overall climatic situation at the end of the last ice age, however, was already similar to the present one, except some displacement of the Intertropical Convergence Zone (ITCZ) due to the more extended ice coverage of the northern hemisphere (Fleitmann & Matter, 2009; Preusser et al., 2002).

Nowadays the ITCZ crosses at its most northern position the Arabian Peninsula so that part of Oman's south is exposed to monsoon during summer and to

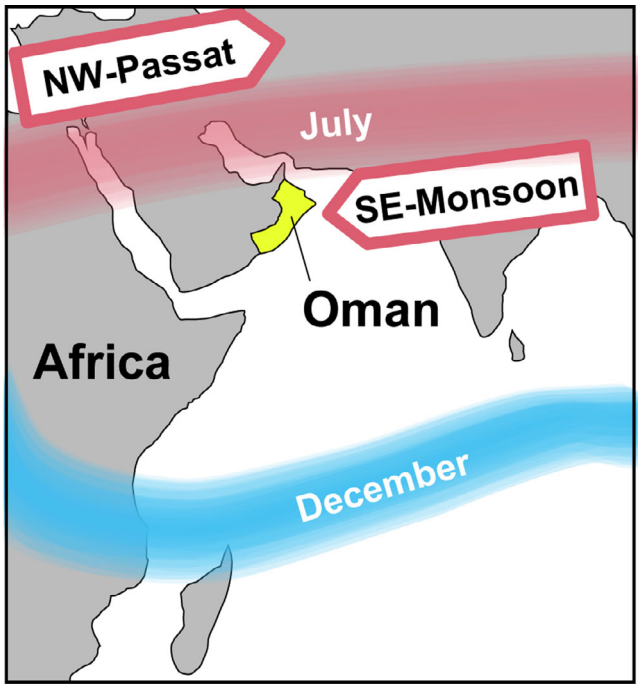

Fig. 7. Wind situation in Oman during summer monsoon and winter Passat (see also Fleitmann et al., 2007). The red and bluish zones mark the Intertropical Convergence Zone. (Color figure can be viewed at wileyonlinelibrary.com.)

Passat during winter time (Fig. 7). These two very distinct weather situations are reflected in Fig. 8 where the high-altitude wind directions at Muscat are shown for 12 months.

An outstanding feature therein is the prevailing wind direction from east (90°) during the summer months. That is what we are looking for, as the curvature of the strewn field, with its deflection to the west at the lower mass end, indicates a wind drift effect from the east. Consequently, as a hypothesis, we adopt a summer monsoon situation for our wind model.

All wind data were taken from the NOAA/ESRL Radiosonde Database Archive (http://www.esrl.noaa.gov/raobs/), now available at http://weather.uwyo.edu/upperair/sounding.html. The Jiddat al Harasis area is roughly halfway between the sounding stations Muscat (#41256) and Salalah (#41316) at distances of 500 km and 350 km, respectively, suggesting an interpolative approach. The sounding data are limited to an altitude of 25 km; at higher altitude, we use extrapolated values, the uncertainties of which, however, have negligible influence. The resulting wind direction model represents consistently the data from both stations (Fig. 9a and 9b). The wind speed, however, is partly higher at Salalah than at Muscat. Data from both stations, merged into one diagram, exhibit a spread of about ±30% in between 9 and 17 km altitude (Fig. 10). To account for this uncertainty, we introduce an additional parameter into the wind model.

Fragmentation Models

A model strewn field produced by a single fragmentation (Fig. 11a) follows a center line with the smaller masses generally staying behind the larger ones due to atmospheric friction. The deceleration is, however, strongly dependent on the drag and shape factors of the fragments thus causing some mass mixing along the line. The curvature of the line may be anything from straight through hockey stick to horseshoe, depending on the wind profile between the fragmentation point and the ground.

Due to considerable transverse velocities from the explosive fragmentation process, the landing points of the fragments will additionally scatter to the left and right of the center line.

With more than one fragmentation, the resulting model strewn field will be an overlap of subfields with similar shapes and converging toward the high mass end. The mass mixing will be therefore stronger both along and across the strewn field. A still rather simple case of this type is a serial fragmentation model (Fig. 11b) where fragments are split off a main body in a series of explosions in decreasing altitudes.

If the meteoroid material is fragile enough, for example, fractured due to heavy shock in space, some fragments may break apart randomly and without explosive fragmentation events (e.g., Tagish Lake, Brown et al., 2002; Innisfree, Halliday et al., 1981; Almahata Sitta, Jenniskens et al., 2009), sometimes down to low altitudes and even during dark flight. That is what we expect from JaH 073 as it contains a network of subparallel shock veins. During drilling of the main mass, the drill cores fell apart at these shock veins (Huber et al., 2008).

With multiple fragmentations, the mass mixing through the strewn field increases still more and the complexity makes a full reconstruction impossible. A multifragmentation model (Fig. 11c) with double or triple fragmentations out of a fragmentation series may, however, serve to explain some special features of a strewn field like outliers.

Upon fragmentation, supposedly via electromagnetic forces (Spurný & Ceplecha, 2008), a part of the kinetic energy associated with the velocity along the trajectory is converted into transverse components. Conservation of momentum favors a release of fragments in opposite directions. In the case of dominating directions other than horizontal or vertical, this may cause an asymmetry of the lateral strewn field extension relative to the center line. Considering the simplest case of a breakup into two halves, one half may be released to the right downward under, for example, 45°, while the other one will head upward to the left. The latter will thus land further ahead

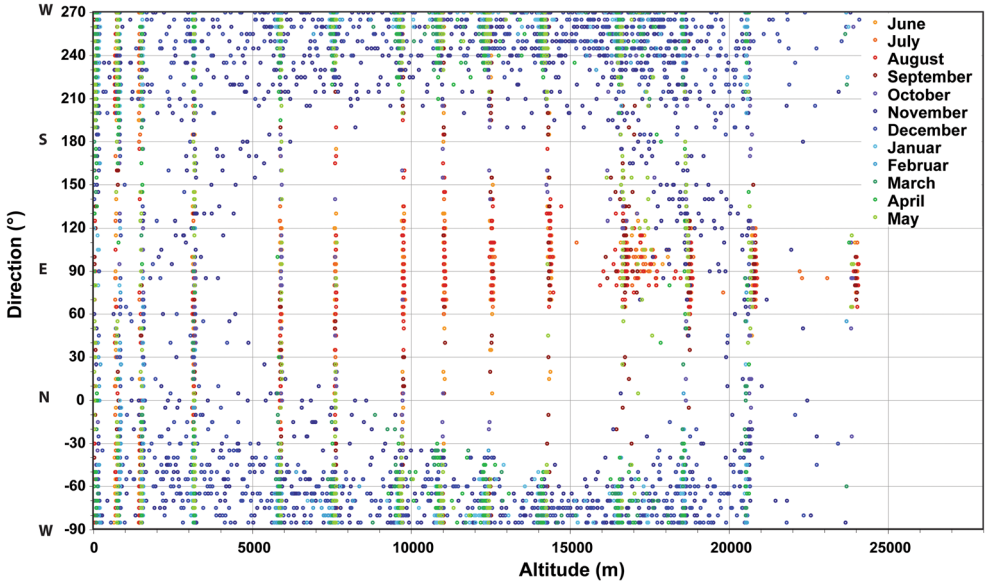

Fig. 8. High altitude wind directions during a period of 12 months at Muscat reflecting two distinct weather situations during summer Monsoon (reddish colors) and winter Passat (bluish colors). Data obtained from the NOAA/ESRL Radiosonde Database Archive, now available at the University of Wyoming (http://weather.uwyo.edu/upperair/sounding.html). (Color figure can be viewed at wileyonlinelibrary.com.)

and left of the strewn field center line than the former on the right side. In combination with multifragmentation, this effect may explain the obvious asymmetry of the JaH 073 strewn field. We tested this hypothesis by modeling selected examples of outliers.

RESULTS AND DISCUSSION

Application of a single fragmentation as proposed by Gnos et al. (2009) yields an already reasonable description of the main parameters of the trajectory (Table 1). The best center line fit is achieved for a fragmentation altitude of about 26 km, which marks the main part of the fragmentation sequence (Fig. 12a). The match of mass group center points with the theoretical masses is good in areas with a close to complete meteorite recovery record. It shows some minor deviations in the vicinity of voids in the strewn field due to geographic features. This is most obvious at the very low mass end.

The single fragmentation model cannot, however, reproduce satisfactorily the transverse mass mixing and especially the width of the strewn field. The model is improved significantly if we allow for a serial fragmentation (Fig. 12b). Most of the strewn field width is explained by four major fragmentations in 34, 26, 22, and 19 km altitude. The geometrical trajectory parameters with the vertical angle at 43 ± 2° and the azimuth at 329 ± 1° do not change beyond the uncertainties (Table 1). The reason is the good statistical database with almost 3500 recovered meteorites from a wide mass range. This holds even with the large uncertainties of the dynamical model parameters as mentioned above due to the evident lack of prehistoric observations. Adjusting the model fit to an entry velocity at the low end of the specified range would increase the fragmentation height by ~2% only.

A closer look to the unexplained rest of the strewn field suggests that there were more fragmentations, also above 34 km and especially below 19 km. However, they are not resolved.

An example for a late fragmentation is the disk-like meteorite 0201-1130 (741 g; Fig. 3) found 1.1 km ahead of the largest mass (stone A in Fig. 1). To understand its extreme location, we have to additionally assume that it was spinning around the normal to the disk (Fig. 3) and moving with the narrow edge ahead (like a flat pebble stone dancing over a water surface); both the exposed cross section and the drag coefficient would then be just right to land it where it was found.

Alternatively, this fragment might have been explained as a split off from a very large undiscovered meteorite of more than 100 kg. The respective area for such a mass was constrained and scrutinized in the field. Nothing was found and, as the probability window for such a mass was small anyway, this scenario was discarded.

In the course of the additional searches, three more outlying meteorites were found to the north: 0902-84 (39.1 g), 0902-85 (169.6 g), and 0902-86 (5800 g) (stones B in Fig. 1). Careful checks showed that these stones

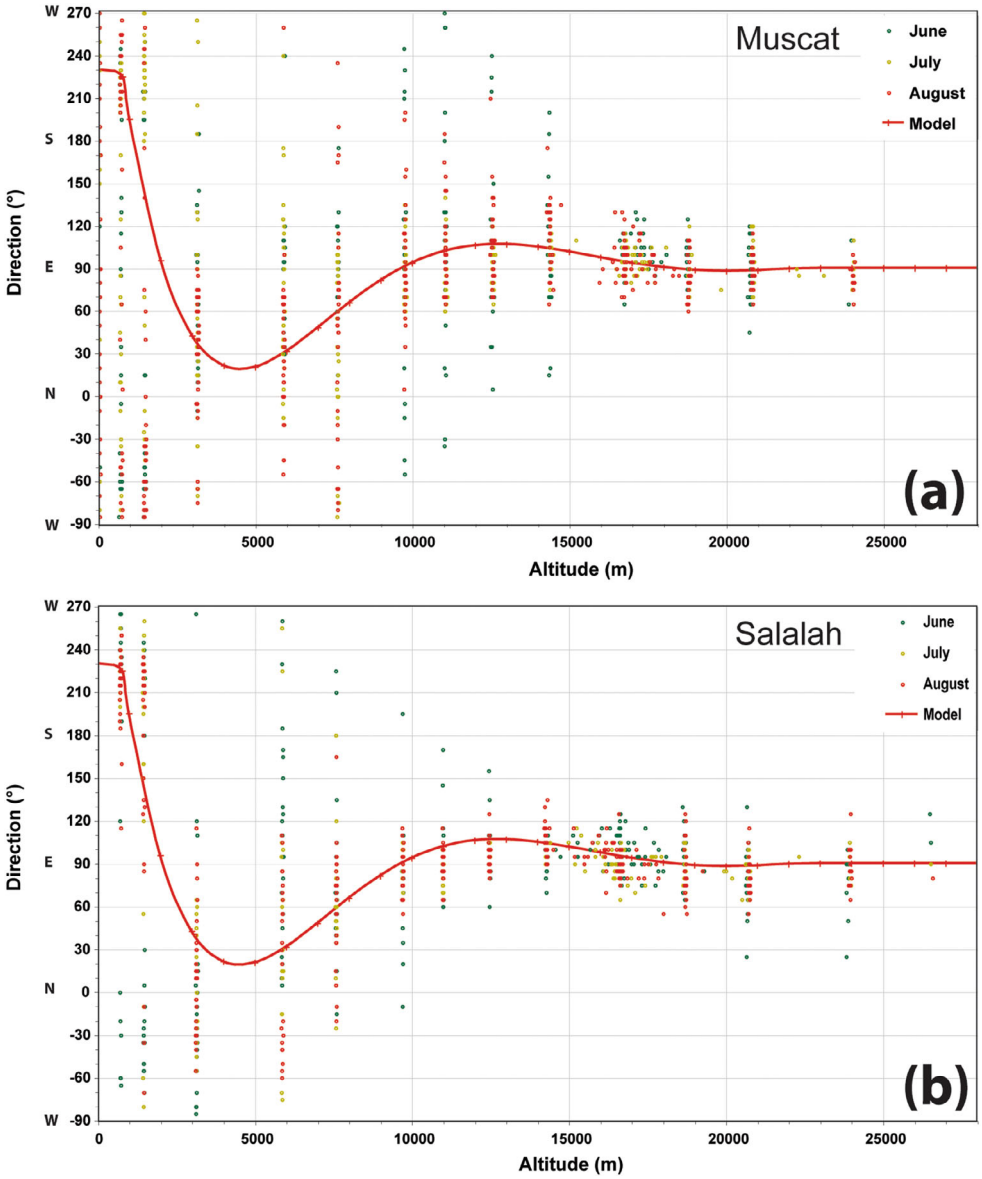

Fig. 9. Wind direction model versus altitude data from Oman sounding stations Muscat (a) and Salalah (b) during summer. (Color figure can be viewed at wileyonlinelibrary.com.)

were part of the strewn field. However, we cannot rule out that the stones were displaced by humans. The 5.8 kg piece could be explained as a product of the secondary fragmentation of a bigger fragment which may have been released violently upward from the main body. The 170 g piece is understood as a very late split off from the 5.8 kg only, which was confirmed later by a check of the matching shapes.

Similarly, the outliers in western direction can be understood by repeated fragmentations adding up the transverse velocity contributions in the same direction that causes the asymmetry as described above. These cases show that only a multifragmentation scenario can explain details of the strewn field.

Considering the large number of fragments, it is not a surprise that they were produced by multifragmentation. Such a fragmentation behavior is indicative for a shocked interior of the meteoroid like with other L6-chondrite falls, for example, Villalbeto in 2004. A still more extreme example is the fall of Chelyabinsk in 2013 with its excessive fragmentation. Despite the fact that the mass of the JaH 073 meteoroid was smaller by more than two orders of magnitude, people living in early Oman 18.1 ka ago must have been witness to a similar spectacular firework.

The successful modeling of the complex strewn field proves that the adopted wind model based on modern data fits surprisingly well. The wind direction is perfectly

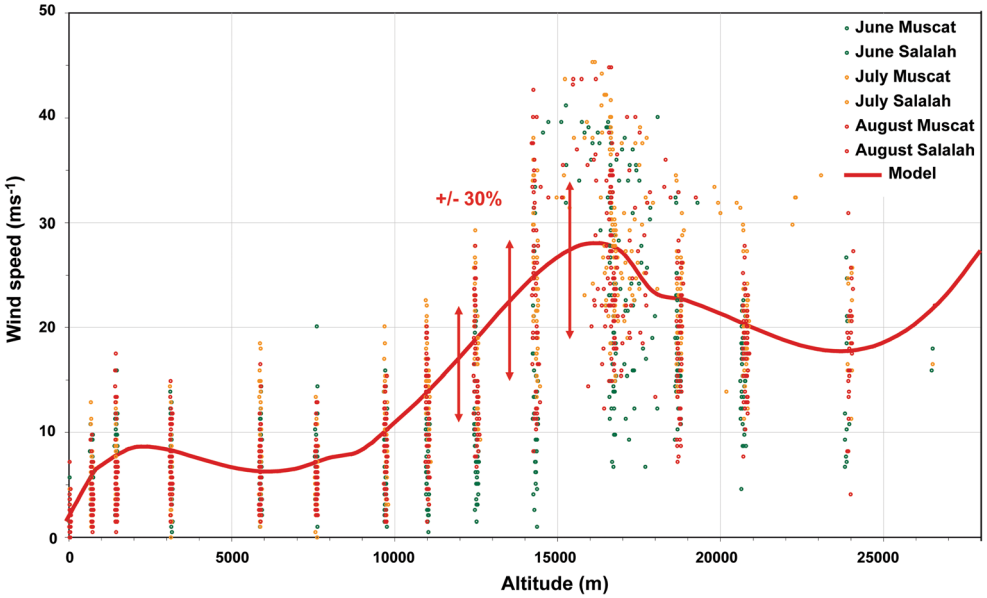

Fig. 10. Wind speed model versus altitude data from sounding stations Muscat and Salalah. Note the increased spread between 9000 and 17,000 m altitude. The best model fit is reached within the lower part of the range, representing Muscat rather than Salalah. (Color figure can be viewed at wileyonlinelibrary.com.)

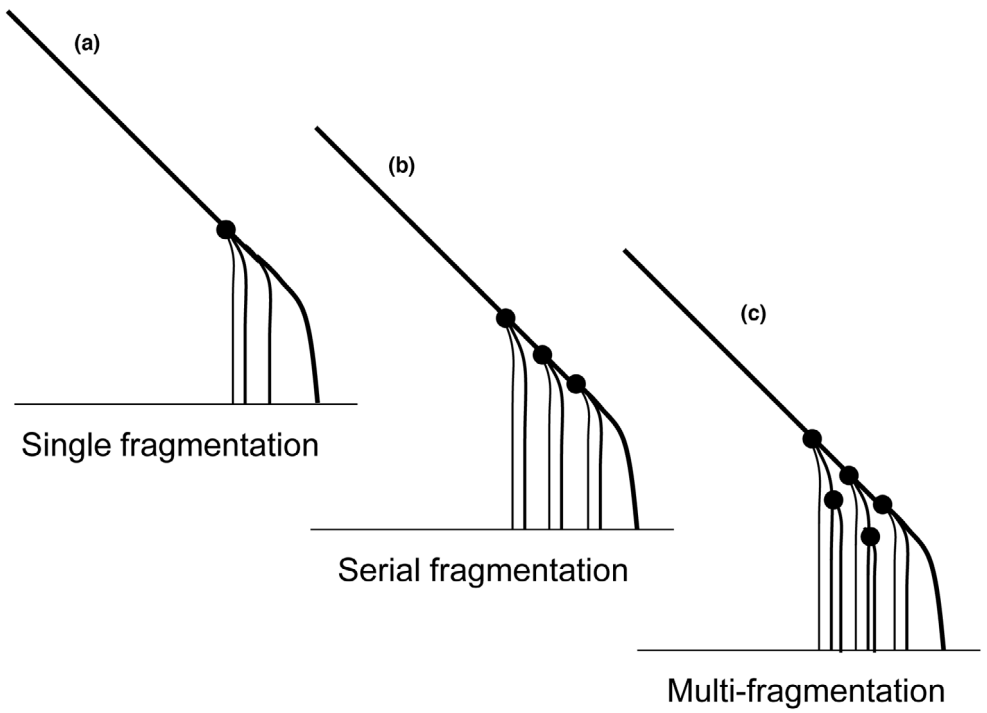

Fig. 11. Fragmentation models with increasing complexity: (a) single fragmentation; (b) serial fragmentation; (c) multifragmentation.

consistent with an average situation in present late July; the wind speed optimum is always within the lower half of the range shown in Fig. 10, being representative for the monsoon in Muscat rather than in Salalah. Therefore, we conclude that the intertropical convergence zone at the end of the last ice age was close to where it is nowadays. To our knowledge, this is the first climate information derived from a meteorite strewn field.

Table 1. Main parameters of the trajectory and the flight model.

Parameter	Value	Range	Comment
Initial altitude	90 km		Assumption, typical range (e.g., Popova et al., 2011)
Initial velocity	20 km s^{-1}	17–23 km s^{-1}	Constrained from mass loss (this work)
Initial mass	12,000 kg	6000–24,000 kg	Constrained from cosmogenic nuclides (Huber et al., 2008)
Trajectory azimuth	329°//330°	±1°//±2°	Multi-/single fragmentation model
Trajectory vertical angle	43°//45°	±2°//±3°	Multi-/single fragmentation model
Fragmentation altitude	26 km	34–19 km	Serial fragmentation around 26 km
Final altitude	12 km	11–13 km	Largest meteorite mass
Length of luminous trajectory	115 km	110–120 km	Based on model assumptions
Meteor duration	7 s	6.5–7.5 s	Based on model assumptions
Dark flight duration	65 s	50–80 s	Largest meteorite mass
Final mass	650 kg	600–700 kg	Extrapolation from recovered meteorites

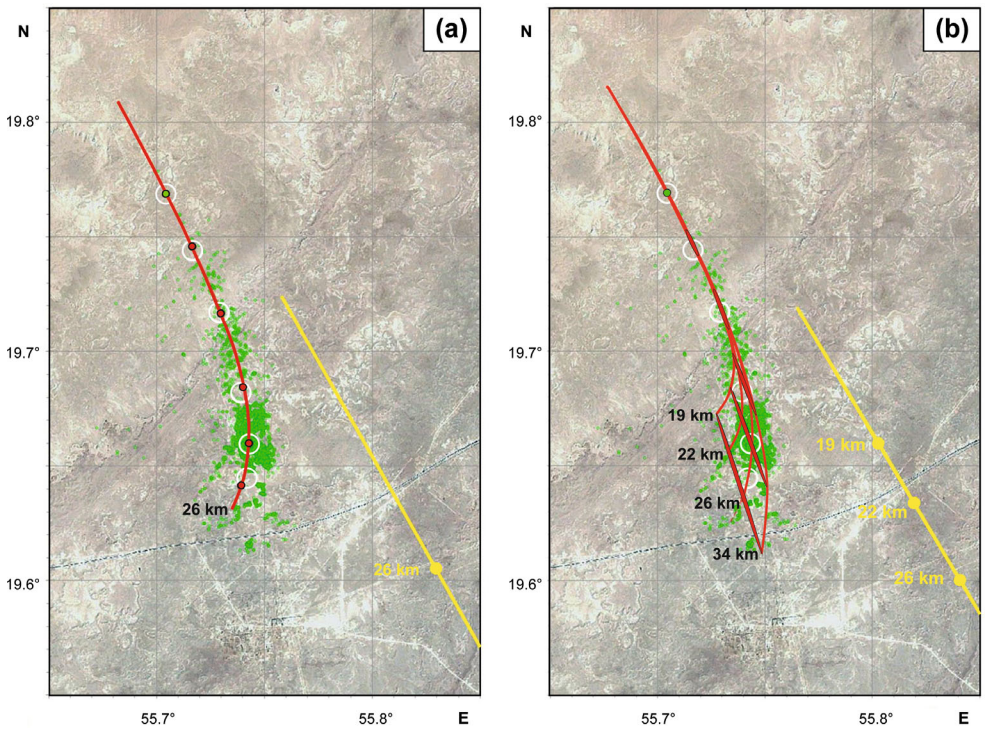

Fig. 12. Strewn field with center lines (red) for fragmentations and final part of the luminous trajectory with fragmentation points (yellow). a) Single fragmentation at 26 km altitude: mass group centers (white circles) versus modeled masses (red points along the strewn line). b) Serial fragmentation with four events between 34 and 19 km altitude (three of four fragmentation points visible): mass group centers (white circles) versus model results (red elongated ellipses combining the modeled masses from the four fragmentations). (Color figure can be viewed at wileyonlinelibrary.com.)

CONCLUSIONS

It is kind of a tradition to describe meteorite strewn fields as "strewn ellipse."

From the discussion above, it is clear that strewn fields may assume many different shapes from perfectly straight to strongly curved depending on wind speed and direction at different altitudes during the fall. Moreover, they may be composed of "sub-fields" depending on the fragmentation sequence, complicating further the overall shape.

In general, a strewn field is widened especially at the high mass end by the transverse speed from fragmentation; at the low mass end, the uncertainty of the wind data increases the width of the expectation area prior to meteorite recovery. Thus, even a straight strewn field may look like a bone rather than an ellipse. Altogether, strewn fields or the respective meteorite expectation areas will virtually never be elliptic. Therefore, it is strongly recommended to avoid the use of the term "strewn ellipse."

It is just the diversity of shapes which makes the analysis of strewn fields attractive and offers the opportunity to acquire interesting information to

- reconstruct data of unobserved falls,
- study fragmentation behavior with implications on material homogeneity,
- shed light on fragmentation mechanism, and
- derive complementary data on climatic, geologic, or other fields.

As a prerequisite for such studies, we encourage the detailed documentation of every single meteorite including outliers, which often play a crucial role in testing the validity and the limits of strewn field modeling.

Acknowledgments—The manuscript is dedicated to three deceased pioneers of meteorite fall observation, Zdenek Ceplecha, Ivan Nemtchinov, and Doug ReVelle, who all commented on the first presentation of this study. Fieldwork in Oman was generously supported by Ali Al Rajhi, Salim Al Busaidi, and Hilal Al Azri from the Public authority for Mining. This work was supported by Swiss National Science Foundation grants 2100-064929, 200020-107681, 200020-119937, and 200021-197247. We thank our main JaH 073 fieldwork colleagues Ali Al-Kathiri, Marc Hauser, Lorenz Moser, Silvio Lorenzetti, Manuel Eggimann, Liliane Huber, and Florian Zurfluh. The manuscript has benefitted from the detailed reviews by Jiri Borovička and Josep Trigo-Rodríguez.

Data Availability Statement—Coordinates and weights of all stones from the strewn field are provided in the supporting information.

Editorial Handling—Dr. Josep M. Trigo-Rodríguez

REFERENCES

Biot, J.-B. 1803. *Relation d'un voyage fait dans le département de l'Orne, pour constanter la réalité d'un météore observé à l'Aigle le 6 floréal an 11*, 1–47. Paris: Baudoin, Imprimeur de l'Institut National.

Bland, P. A., Spurný, P., Towner, M. C., Bevan, A. W., Singleton, A. T., Bottke, W. F., Jr., Greenwood, R. C., et al. 2009. An Anomalous Basaltic Meteorite from the Innermost Main Belt. *Science* 325: 1525–7.

Borovička, J., Spurný, P., Brown, P. G., Wiegert, P., Kalenda, P., Clark, D., and Shrbeny, L. 2013. The Trajectory, Structure, and Origin of the Chelyabinsk Asteroidal Impactor. *Nature* 503: 235–7.

Britt, D. T., and Consolmagno, G. J. 2003. Stony Meteorite Porosities and Densities: A Review of the Data Through 2001. *Meteoritics & Planetary Science* 38: 1161–80.

Brown, P. G., ReVelle, D. O., Tagliaferri, E., and Hildebrand, A. R. 2002. An Entry Model for the Tagish Lake Fireball Using Seismic, Satellite and Infrasound Records. *Meteoritics & Planetary Science* 37: 661–75.

Buhl, S., and Wimmer, K. 2013. Chelyabinsk Superbolide: Strewn Field Map and Ground Projection of Trajectory. http://www.meteorite-recon.com/home/meteorite-documentaries/chelyabinsk-superbolide/p6. Accessed November 06, 2022.

Ceplecha, Z. 1961. Multiple Fall of Přibram Meteorites Photographed. *BAICz* 12: 21–46.

Ceplecha, Z., Borovička, J., Elford, W. G., ReVelle, D., Hawkes, R. L., Porubčan, V., and Šimek, M. 1998. Meteor Phenomena and Bodies. *Space Science Reviews* 84: 327–471.

Ceplecha, Z., Spurný, P., Borovička, J., and Keclikova, J. 1993. Atmospheric Fragmentation of Meteoroids. *Astronomy and Astrophysics* 279: 615–26.

Clarke, R. S., Jarosewich, E., Mason, B., Nelen, J., Gomez, M., and Hyde, J. R. 1970. The Allende, Mexico, Meteorite Shower. *Smithsonian Contributions to the Earth Sciences* 5: 1–53.

Cleverly, W. H., Jarosewich, E., and Mason, B. 1986. Camel Donga Meteorite, a New Eucrite from the Nullarbor Plain, Western Australia. *Meteoritics* 21: 263–81.

Colas, F., Zanda, B., Bouley, S., Jeanne, S., Malgoyre, A., Birlan, M., Blanpain, C., et al. 2020. FRIPON: A Worldwide Network to Track Incoming Meteoroids. *Astronomy & Astrophysics* 644: A53.

De Laeter, J. R. 1972. The Munderabilla Meteorite Shower. *Meteoritics* 7: 285–94.

De Laeter, J. R., and Cleverly, H. 1983. Further Finds from the Munderabilla Meteorite Shower. *Meteoritics* 18: 29–34.

Devillepoix, H. A. R., Cupák, M., Bland, P. A., Sansom, E. K., Towner, M. C., Howie, R. M., Hartig, B. A. D., et al. 2020. A Global Fireball Observatory. *Planetary and Space Science* 191: 105036.

Devillepoix, H. A. R., Sansom, E. K., Shober, P., Anderson, S. L., Towner, M. C., Lagain, A., Cupák, M., et al. 2022. Trajectory, Recovery, and Orbital History of the Madura Cave Meteorite. *Meteoritics & Planetary Science* 57: 1328–38.

Emel'Yananko, V. V., Naroenkov, S. A., Jenniskens, P., and Popova, O. P. 2014. The Orbit and Dynamical Evolution of the Chelyabinsk Object. *Meteoritics & Planetary Science* 49: 2169–74.

Fleitmann, D., Burns, S. J., Mangini, A., Mudelsee, M., Kramers, J., Villa, I., Neff, U., et al. 2007. Holocene ITCZ and Indian Monsoon Dynamics Recorded in Stalagmites from Oman and Yemen (Socotra). *Quaternary Science Reviews* 26: 170–88.

Fleitmann, D., and Matter, A. 2009. The Speleothem Record of Climate Variability in Southern Arabia. *Comptes Rendus Geoscience* 341: 633–42.

Foote, W. M. 1912. Preliminary Note on the Shower of Meteoric Stones near Holbrook, Navajo County, Arizona, July 19, 1912. *American Journal of Science* 34: 437–56.

Fuchs, L. H., Olson, E., and Jensen, K. J. 1973. Mineralogy, Mineral-Chemistry and Composition of the Murchison (C2) Meteorite. *Smithsonian Contributions to the Earth Sciences* 10: 1–39.

Gnos, E., Eggimann, M., Al-Kathiri, A., and Hofmann, B. A. 2006. The JaH 091 Strewnfield. *Meteoritics & Planetary Science* 41: 5112.

Gnos, E., Lorenzetti, S., Eugster, O., Jull, A. J. T., Hofmann, B. A., Al-Kathiri, A., and Eggimann, M. 2009. The Jiddat al Harasis 073 Strewnfield, Sultanate of Oman. *Meteoritics & Planetary Science* 44: 375–87.

Grossman, J. N. 2000. The Meteoritical Bulletin, 84. *Meteoritics & Planetary Science* 36: A199–225.

Halliday, I. 1971. Photographic Fireball Networks. In *Evolutionary and Physical Properties of Meteoroids*, edited

by C. L. Hemenway. NASA SP-319, 1–8. Cambridge: Cambridge University Press.
Halliday, I., Griffin, A. A., and Blackwell, A. T. 1981. The Innisfree Meteorite Fall: A Photographic Analysis of Fragmentation, Dynamics and Luminosity. *Meteoritics* 16: 153–70.
Huber, L., Gnos, E., Hofmann, B., Welten, K. C., Nishiizumi, K., Caffee, M. W., Hillegonds, D. J., and Leya, I. 2008. The Complex Exposure History of the Jiddat al Harasis 073 l-Chondrite Shower. *Meteoritics & Planetary Science* 43: 1691–708.
Jenniskens, P., Betlem, H., Betlem, J., Barifaijo, E., Schlueter, T., Hampton, C., Laubenstein, M., Kunz, J., and Heusser, G. 1994. The Mbale Meteorite Shower. *Meteoritics* 29: 246–54.
Jenniskens, P., Shaddad, M. H., Numan, D., Elsir, S., Kudoda, A. M., Zolensky, M. E., Le, L., et al. 2009. The Impact and Recovery of Asteroid 2008 TC3. *Nature* 458: 485–8.
Jenniskens, P., Utas, J., Yin, Q.-Z., Matson, R. D., Fries, M., Howell, J. A., Free, D., et al. 2019. The Creston, California, Meteorite Fall and the Origin of L Chondrites. *Meteoritics & Planetary Science* 54: 699–720.
Jilin Consortium Study. 1985. Eight Papers on the Jilin Meteorite. *Earth and Planetary Science Letters* 72: 246–310.
Koch, A. 1882. Bericht über den am 3. Februar l. J. Stattgefundenen Meteoritenfall von Mócs in Siebenbürgen. *Sitzungsberichte der mathematisch-naturwissenschaftliche Classe der Kaiserlichen Akademie der Wissenschaften* 85/1: 116–32.
Kring, D. A., Jull, A. J. T., McHargue, L. R., Bland, P. A., Hill, D. H., and Berry, F. J. 2001. Gold Basin Meteorite Strewn Field, Mojave Desert, Northwest Arizona: Relic of a Small Late Pleistocene Impact Event. *Meteoritics & Planetary Science* 36: 1057–66.
Krinov, E. L. 1966. *Giant Meteorites*. Oxford: Pergamon Press. 397.
LaPaz, L. 1965. Catalog of the Collections of the Institute of Meteoritics, the University of New Mexico. *Meteoritics & Planetary Science* 45: 1638–56.
Moore, L. B., Flynn, G. J., and Clock, W. 1999. Density and Porosity Measurements on Meteorites: Implications for the Porosities of Asteroids (Abstract #1128). 30th Lunar and Planetary Science Conference. CD-ROM.
Oberst, J., Molau, S., Heinlein, D., Gritzner, C., Schindler, M., Spurný, P., Ceplecha, Z., Rendtel, J., and Betlem, H. 1998. The European Fireball Network: Current Status and Future Prospects. *Meteoritics & Planetary Science* 33: 49–56.
Popova, O., Borovička, J., Hartmann, W. K., Spurný, P., Gnos, E., Nemtchinov, I., and Trigo-Rodríguez, J. M. 2011. Very Low Strengths of Interplanetary Meteoroids and Small Asteroids. *Meteoritics* 46: 1525–50.
Popova, O., Jenniskens, P., Emel'yanenko, V., Kartashova, A., Biryukov, E., Khaibrakhmanaov, S., Shuvalov, V., et al. 2013. Chelyabinsk Airburst, Damage Assessment, Meteorite Recovery, and Characterization. *Science* 342: 1069–73.
Preusser, F., Radies, D., and Matter, A. 2002. A 160′000-Year Record of Dune Development and Atmospheric Circulation in Southern Arabia. *Science* 296: 2018–20.
Schlüter, J., Schultz, L., Thiedig, F., Al-Mahdi, B. O., and Abu Aghreb, A. E. 2002. The Dar al Gani Meteorite Field (Libyan Sahara): Geological Setting, Pairing of Meteorites, and Recovery Density. *Meteoritics & Planetary Science* 37: 1079–93.
Simon, S. B., Wacker, J. F., Clayton, R. N., Mayeda, T. K., Schwande, J. R., Sipiera, P. P., Grossman, L., and Wadhwa, M. 2004. The Fall, Recovery and Classification of the Park Forest Meteorite. *Meteoritics & Planetary Science* 39: 625–34.
Sliz, M. U., Hofmann, B. A., Leya, I., Szidat, S., Espic, C., Gattacceca, J., Braucher, R., Borschnek, D., Gnos, E., and ASTER Team. 2022. Terrestrial Ages of Seven Meteorite Strewn Fields and Two Single Unpaired Meteorites from the Sultanate of Oman Determined Using ^{14}C and ^{10}Be. *Meteoritics & Planetary Science*.
Spurný, P., Bland, P., Shrbený, L., Borovička, J., Ceplecha, Z., Singelton, A., Bevan, A. W. R., et al. 2012. The Bunburra Rockhole Meteorite Fall in SW Australia: Fireball Trajectory, Luminosity, Dynamics, Orbit, and Impact Position from Photographic and Photoelectric Records. *Meteoritics & Planetary Science* 47: 163–85.
Spurný, P., Bland, P. A., Borovička, J., Shrbený, L., McClafferty, T., Singelton, A., Bevan, A. W. R., Vaughan, D., Towner, M. C., and Deacon, G. 2009. The Bunburra Rockhole Meteorite Fall in SW Australia: Determination of the Fireball Trajectory, Luminosity and Impact Position from Photographic Records (Abstract #1498). 40th Lunar and Planetary Science Conference. CD-ROM.
Spurný, P., and Ceplecha, Z. 2008. Is Electric Charge Separation the Main Process for Kinetic Energy Transformation into the Meteor Phenomenon? *Astronomy & Astrophysics* 489: 449–54.
Trigo-Rodríguez, J. M., Dergham, J., Gritsevich, M., Lyytinen, E., Silber, E. A., and Williams, I. P. 2021. A Numerical Approach to Study Ablation of Large Bolides: Application to Chelyabinsk. *Advances in Astronomy* 2021: 8852772.
Welten, K. C., Caffee, M. W., Hillegonds, D. J., McCoy, T. J., Masarik, J., and Nishiizumi, K. 2011. Cosmogenic Radionuclides in L5 and LL5 Chondrites from Queen Alexandra Range, Antarctica: Identification of a Large L/LL5 Chondrite Shower with a Preatmospheric Mass of Approximately 50,000 kg. *Meteoritics & Planetary Science* 46: 177–98.
Wimmer, K. 2009. Studies of Meteorite Drag-Shape Factors During Dark Flight. Bolides and Meteorite Falls, Prague, May 10–15, Abstract, p. 25.
Wright, S. P., Vesconi, M. A., Gustin, A., Williams, K. K., Ocampo, A. C., and Cassidy, W. A. 2006. Revisiting the Campo del Cielo, Argentina Crater Field: A New Data Point from a Natural Laboratory of Multiple Low Velocity, Oblique Impacts (Abstract #1102). 37th Lunar and Planetary Science Conference. CD-ROM.

SUPPORTING INFORMATION

Additional supporting information may be found in the online version of this article.

Data S1. Coordinates and weights for stones of the JaH 073 strewn field.